Influence of Precipitation Method on Acid-Base Catalyzed Reactions over Mg-Zr Mixed Oxides

Joseph T. Kozlowski[a], Malte Behrens[b], Robert Schlögl[b] and Robert J. Davis[b]*

[a] Department of Chemical Engineering, University of Virginia

102 Engineers' Way, Charlottesville, VA 22904

[b] Fritz-Haber-Institut der Max-Planck-Gesellschaft

Faradayweg 4-6, 14195 Berlin, Germany

*Corresponding Author. E-mail Address: rjd4f@virginia.edu

Keywords: aldol reaction, heterogeneous catalysis, microcalorimetry, transesterification, ethanol coupling, magnesia

Table of Contents Abstract

Mixed oxides of Zr and Mg were prepared by two precipitation methods to investigate the promotional effect of ZrO_2 on MgO for dehydration, dehydrogenation, aldolization and transesterification. The oxide catalysts were characterized by adsorption microcalorimetry, electron microscopy and X-ray diffraction, and results were correlated to catalytic performance.

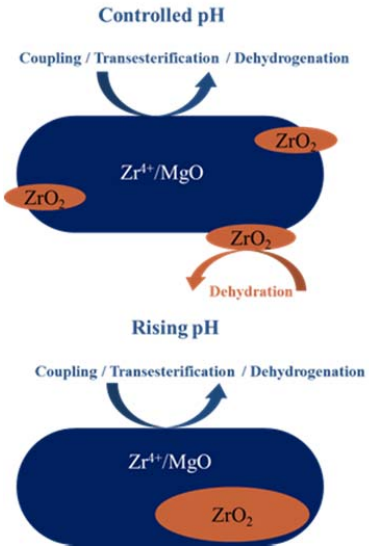

Abstract

To examine the promotional effect that zirconia has on magnesia, mixed oxides were prepared by co-precipitation under controlled pH conditions or rising pH conditions. The resulting mixed oxides were characterized using NH_3 and CO_2 adsorption microcalorimetry, X-ray diffraction, and scanning electron microscopy. The samples were also tested as catalysts for transesterification of tributyrin with methanol, coupling of acetone and conversion of ethanol to ethene, ethanal and butanol. Zirconia promoted the activity of MgO for both transesterification and acetone coupling, presumably by exposing new acid-base pairs at the surface. During ethanol conversion, however, zirconia promoted the dehydration reactions. Characterization and reactivity results suggest that a Mg:Zr sample prepared by constant pH precipitation exposes more ZrO_2 than a sample prepared by the rising pH method.

Introduction

Promotion of the classical solid base catalyst MgO by addition of amphoteric ZrO_2 has been recognized for many years.[1–8] For example, mixed oxides of MgO and ZrO_2 have been employed as catalysts and catalyst supports for reactions such as aldol condensation,[3,9] transesterification,[4,5] alcohol dehydration and alcohol dehydrogenation.[10,11] Both aldol condensation[3,12,13] and alcohol dehydrogenation[14,15] are claimed to be accelerated over materials with acid-base pairs (amphoteric materials) compared to traditional solid bases, which may account for the catalytic effectiveness of Mg:Zr mixed oxides. To properly investigate mixed oxides for reactions involving acid-base pairs, materials need to be properly prepared to expose the desired components. In this work, two different methods of synthesizing Mg:Zr mixed oxides will be compared for both sample uniformity and surface functionality.

The common solid base MgO has been explored extensively using many different techniques, including IR spectroscopy of adsorbed molecular probes,[16–20] adsorption microcalorimetry,[4,21,22] temperature-programmed desorption,[1,23–26] catalytic probe reactions,[20,23,24,27] electron microscopy,[25,26,28,29] and quantum chemical calculations.[18,30–37] These experimental and theoretical methods have provided a thorough understanding of the surface basicity and its structural origins in MgO. Many of these same techniques can also be used to probe the properties of Mg:Zr mixed oxides.

One way to quantify the acid and base sites on a material is to measure the heat of adsorption and the chemisorption capacity of ammonia and carbon dioxide, respectively, by adsorption microcalorimetry.[4,22,38,39] In this work, we will attempt to correlate the acid-base properties of the mixed oxides with structural features evaluated by the electron microscopy and X-ray diffraction. Although the physical characteristics are good indicators of surface reactivity,

the ultimate test is performance in a catalytic reaction. Therefore, multiple catalytic reactions will be used to probe Mg:Zr mixed oxides.

As mentioned earlier, transesterification has been widely studied over magnesia and magnesia-containing materials,[4,5,28,40–42] and prior work in our lab has confirmed the positive influence of Zr on MgO-catalyzed transesterification of tributyrin with methanol. Since MgO is well understood and has been evaluated thoroughly for transesterification, it is a reaction that can be used to probe the surface acid-base properties of related materials.

Acetone coupling, or aldol condensation of two acetone molecules, has also been studied over a wide variety of materials with particular attention paid to MgO. As with transesterification, acid-base bifunctional materials appear to be more effective catalysts than traditional solid bases for aldol condensation.[12,13,43] Some examples of acid-base bifunctional catalysts for aldol condensation include: Y/MgO,[44] Mg:Al mixed oxides,[43,45–47] amorphous aluminophosphate,[13] Cs/ZrO_2,[12] and Mg:Zr mixed oxides catalysts.[3,9] In many of these studies, a goal of the preparation was to locate a Lewis acid center in proximity to a strong base site. It is important to recognize, though, an increase in reactivity may not be exclusively the result of acid-base bifunctionality, but also may arise from a change in base site density and base site strength.

The reactions of alcohols can also be used to probe the acid-base character of mixed oxides.[10,20,44,48] Although alcohols can both dehydrate and dehydrogenate, the carbonyl product of dehydrogenation can also couple to form a heavier alcohol over suitable catalysts. Ethanol is of interest since the coupling product is butanol, which is of higher value.[14,49–56] While MgO has been studied quite extensively for ethanol reactivity,[14,51–53,56] the relative rates of ethene,

ethanal, and butanol formation can provide information on the surface acid and base properties of the Mg:Zr mixed oxide catalysts.

In this study, a Mg:Zr mixed oxide is synthesized via a constant pH precipitation method with the intent of producing a highly uniform sample that can be compared to a traditionally-precipitated Mg:Zr mixed oxide formed by increasing the pH during precipitation. Scanning electron microscopy and X-ray diffraction were performed on the mixed oxide catalysts to compare how the synthesis method impacted the sample morphology. Results from ammonia and carbon dioxide adsorption microcalorimetry, as well as rates from tributyrin transesterification with methanol, acetone coupling, and ethanol conversion, were correlated to morphological properties to elucidate how sample preparation can influence surface reactivity.

Results

Catalyst Characterization

Synthesis of Mg:Zr mixed oxides by the rising pH precipitation method can create non-uniform distributions of the two oxides in the final material.[3] Therefore, we desired to compare the physical properties and catalytic effectiveness of the materials prepared at constant pH to those prepared by the rising pH method. Figure 1 shows the pH in a Labmax reactor throughout the synthesis of a Mg:Zr 11:1 mixed oxide and confirmed that the precipitation occurred at a constant pH of 10.5.

Table 1 summarizes the compositions of all the materials prepared in this work. It should be noted that all the materials prepared by the rising pH precipitation method, except for the Mg on Zr 11:1 sample, are the same ones presented in Kozlowski et al.[4] Residual Na levels were evaluated since alkali metals will influence the acid-base properties of the solids. In all cases,

the Na level was lower than 350 ppm, with the majority of samples having less than 100 ppm Na. In prior work, Na loadings below 1,000 ppm had a negligible effect on reactivity in the transesterification of tributyrin with methanol. Measured ratios of Mg:Zr were close to the nominal values, illustrating the effectiveness of the precipitation.

In Figure 2, diffraction patterns are presented for the Mg:Zr 11:1 samples prepared by controlled pH precipitation and rising pH precipitation, as well as for MgO supported on ZrO_2 (11:1). The MgO on ZrO_2 sample shows peaks for both crystalline magnesia and zirconia (tetragonal and monoclinic). A Scherrer analysis of the tetragonal zirconia phase for the rising and controlled pH samples gave crystallite sizes of about 10 and 8.6 nm respectively.

The XRD results indicated that the controlled pH precipitated material had slightly smaller crystallites of zirconia compared to the rising pH precipitated catalyst, which was confirmed by microscopy. Scanning electron microscopy was performed on both the controlled pH precipitation and rising pH precipitation samples and a few example images and line scans for the two materials are shown in Figures 3 and 4. The difference in the uniformity between the two samples is quite apparent in the SEM images and in the EDX line scans of the two samples. The sample prepared by the rising pH method had larger domains of zirconia, and these domains appeared to be highly concentrated within each particle. The controlled precipitation sample showed a more uniform particle size and smaller domains of zirconia. These observations are consistent with the expected increase in sample uniformity achieved by the controlled pH precipitation method. While we were able to observe the morphology and size of zirconia domains by SEM, we could not distinguish if large regions of zirconia were exposed on the surface or if they were covered with thin layers of MgO. To help quantify the surface

concentration of zirconia (which is more acidic and less basic than MgO) the acid and base properties of the materials were evaluated.

The acid and base sites were probed by adsorption microcalorimetry of ammonia and carbon dioxide on the two Mg:Zr 11:1 samples as well as on zirconia and magnesia prepared by controlled pH precipitation. The adsorption isotherms and differential heats of adsorption are shown in Figures 5 and 6 for carbon dioxide and ammonia, respectively. A summary of the initial heats of adsorption and saturation coverages is presented in Table 2.

Although zirconia and magnesia have similar uptakes of CO_2, MgO exhibited stronger interactions with the weakly acidic probe molecule as indicated by the higher heat of adsorption (162 vs 123 kJ mol^{-1}). Very different results were found with NH_3 adsorption microcalorimetry. Figure 6 and Table 2 clearly illustrate the much higher capacity of ZrO_2 surfaces for NH_3 compared to MgO (3.5 vs 0.70 μmol m^{-2}) and a much higher initial heat of adsorption (170 vs 120 kJ mol^{-1}).

Even though zirconia was present in the Mg:Zr 11:1 mixed oxide sample in low concentration (8.2 at.% in the rising pH sample and 5.8 at.% in the controlled precipitation sample), exposed Zr cations are still anticipated to significantly influence the ammonia adsorption isotherms since zirconia has a much stronger interaction and overall capacity for NH_3 compared to magnesia. For zirconia, 3.5 μmol m^{-2} of ammonia was adsorbed on exposed Zr cations present at a maximum surface density of 16.6 μmol m^{-2} based on the (111) surfaces of tetragonal zirconia.[57] We assume that the quantity of ammonia adsorbed on Brønsted acid sites is much lower than that on Lewis acid sites because of the high temperature used in the sample pretreatment. Prior work on a tetragonal zirconia with a thermal pretreatment similar to the

samples in this study revealed only Lewis acid sites evaluated by IR spectroscopy of adsorbed pyridine.[57] The maximum theoretical capacity for ammonia based on crystallographic parameters can be used to compare MgO and ZrO_2. For magnesia, 0.7 μmol m^{-2} of ammonia was adsorbed. Since MgO is a solid base, the weak interaction of NH_3 with the surface likely arises from hydrogen-bonding interactions and possibly NH_3 dissociation by strongly basic oxygen atoms. For example, Tsyganenko et al. reported that ammonia adsorbed on MgO evacuated at greater than 723 K was either hydrogen bonded to surface O^- anions or dissociated into surface bound amide and hydroxyl groups,[58] indicating ammonia adsorption on MgO is likely to involve surface oxygen groups. Based on the (100) surface in MgO there are 9.37 μmoles m^{-2} of O ions. This would indicate that zirconia has higher capacities per maximum theoretically exposed adsorption site and much stronger affinity for ammonia than magnesia. The Mg:Zr 11:1 sample prepared by rising pH presents few acid sites, with none having $-\Delta H_{ads}$ greater than about 85 kJ mol^{-1} (Figure 6). The mixed oxide sample prepared by controlled precipitation also exhibited few sites for ammonia adsorption, but nearly half of the adsorption sites had a $-\Delta H_{ads}$ greater than 100 kJ mol^{-1}, with some sites having $-\Delta H_{ads}$ greater than those on MgO. Evidently, the controlled pH precipitation method formed a sample exposing surfaces with a higher density of zirconia compared to a sample prepared by the traditional rising pH method.

Transesterification of Tributyrin with Methanol

The rate of transesterification of tributyrin with methanol was used to compare a sample prepared by controlled pH precipitation to that prepared by increasing the pH. A summary of the rate constants for the initial transesterification of tributyrin to dibutyrin (k_1) is provided in Table 3. The Mg:Zr 11:1 sample prepared by controlled precipitation catalyzed the rate of transesterification similar to that over Mg:Zr 11:1 prepared by the rising pH method, which was

several times greater than the rate over MgO. It should be noted that ZrO_2 was not active for the reaction under these conditions. Mixed oxide samples containing greater amounts of ZrO_2 were similar to, or less active, than pure MgO.

To further explore how the interface between the two phases (MgO and ZrO_2) might be involved in the promotion of the reaction, a sample in which MgO was deposited onto ZrO_2 was synthesized. This sample showed both MgO and ZrO_2 by XRD, however it did not promote the transesterification of tributyrin with methanol because the surface area normalized rate constant was below that of pure MgO.

A likely explanation for the observed promotional influence of Zr is that appropriate strength acid-base pairs are present on the mixed oxide surface. To evaluate these materials for acid-base bifunctionality, a reaction such as acetone coupling was performed since it has been proposed to occur faster over bifunctional materials.[15]

Acetone Coupling and Condensation

The pure and mixed oxide materials were used in acetone coupling at 299 K to produce diacetone alcohol. The rates of diacetone alcohol production, normalized to the total surface area of a sample, are presented in Table 4. Similar to the results from transesterification, the Mg:Zr 11:1 mixed oxides showed a higher rate (nearly double) compared to MgO, whereas ZrO_2 was inactive. The inactivity of zirconia at 299 K is consistent with the work of Zaki et al.[59] Using IR spectroscopy, they observed acetone adsorbed on Lewis acid sites, but found little evidence for acetone coupling products. The lack of coupling products on the surface at room temperature is likely the results of zirconia's rather weak basicity since higher temperatures are needed to activate acetone.[59] To address this issue, we studied acetone condensation reactions at elevated

temperature. The reactivity results from acetone conversion at 573 K are reported in Table 5. Mesityl oxide was the major condensation product observed over all of the catalysts.

A prior report has indicated that addition of Y^{3+} to MgO increases deactivation since the more Lewis acidic metal ion helps stabilize reaction intermediates that lead to acetone coupling products. In our study with MgO and ZrO_2 mixed oxides, all samples containing MgO deactivated quickly. In fact, initial conversions reported in Table 5 are quite likely influenced by the rapid deactivation at very short times on stream. On the other hand, acetone condensation over zirconia proceeded without substantial deactivation, revealing only a 10% decrease in rate over 12 h of reaction (Table 5).

Ethanol Reactivity

The observed promotion of transesterification and low temperature coupling of acetone over Mg:Zr mixed oxides compared to MgO led us to explore their potential for Guerbet coupling of alcohols. Therefore, ethanol conversion at 673 K was evaluated in a flow reactor. Ethanol can dehydrate to ethene, dehydrogenate to ethanal and couple to heavier products such as butanol and higher alcohols. The rates at 683 K for dehydration, dehydrogenation and Guerbet coupling of ethanol are presented in Table 6. As expected, zirconia catalyzed dehydration faster than MgO or Mg:Zr 11:1 mixed oxides by more than an order of magnitude, presumably because of the stronger acidity of ZrO_2 compared to MgO. Thus, ethanol dehydration should be a very sensitive probe for Zr^{4+} at the surface of the mixed oxide. The Mg:Zr 11:1 sample prepared by the rising pH method exhibited a lower rate of dehydration compared to the mixed oxide prepared by controlled precipitation. This is consistent with the results presented earlier that suggested the sample prepared by the rising pH method exposed less

zirconia than the mixed oxide prepared by the controlled pH precipitation method. In Table 7, the TOFs for ethanol dehydration, normalized by the ammonia uptake (Table 2), and ethanol dehydrogenation, based on the carbon dioxide uptake (Table 2), are presented. The substantial variation in TOF for dehydration indicates that total ammonia uptake is not a good basis for normalizing dehydration rates. The rate appears to also depend on the strength of the acid sites. In contrast, the relatively constant value of TOF for dehydrogenation suggests that CO_2 adsorption capacity might be a reasonable basis for normalization.

Discussion

Results from several physical and chemical probes reveal the complex nature of the mixed oxides of Mg and Zr. Although controlled pH precipitation of Zr and Mg gave a more even distribution of Zr throughout the sample and smaller ZrO_2 crystallites, compared to a mixed oxide prepared by a rising pH method, the fraction of exposed ZrO_2 was greater with controlled precipitation. Since Zr precipitates at a lower pH than Mg, the rising pH method would favor the initial precipitation of the zirconium followed by subsequent precipitation/deposition of magnesium. This sequence of reactions would give particles that are more MgO-rich at the surface, which is consistent with adsorption and reaction results. Additionally, mixed oxides prepared by a rising pH method have been shown to expose an MgO like surface based on DRIFTS of methanol and carbon dioxide adsorption.[4]

A proposed simple diagram of the surface of these materials is shown in Figure 7. For the controlled precipitation method, two regions are exposed, 1. small zirconia crystallites, although inactive for aldol condensation and transesterification, can be probed by ammonia microcalorimetry and higher ethanol dehydration rates, and 2. crystallites of mostly magnesia

with small amounts of zirconium. The presence of isolated Zr with MgO could account for the increase in reactivity as well as the increase in the heat of carbon dioxide adsorption and would be consistent with the work of Sádaba et al.[3] While the sample prepared with rising pH would also have these domains of isolated Zr with MgO, it would have less exposed crystalline zirconia and therefore a lower heat of ammonia adsorption and a lower ethanol dehydration rate.

Conclusions

A mixed oxide of Mg:Zr 11:1 that was prepared in a controlled precipitation had a higher surface exposure of zirconia than a material prepared traditionally by increasing the pH. Although the controlled precipitation method produced a more uniform distribution of zirconia, the larger surface exposure of zirconia caused an undesirable increase in the rate of ethanol dehydration, which is detrimental to the Guerbet coupling reaction. Since ZrO_2 was inactive for transesterification and low temperature coupling of acetone, the presence of small amounts of crystalline ZrO_2 on the surface of Mg:Zr 11:1 was not detrimental to those reactions. In contrast, Mg:Zr 11:1 mixed oxides prepared by either method were substantially more active for transesterification and low temperature acetone coupling compared to MgO (on a surface area basis). The promotion of MgO-catalyzed reactions by the addition of Zr^{4+} was presumably the result of additional acid-base surface sites that facilitate those reactions.

In summary, both methods of preparation, i.e. controlled precipitation and rising pH precipitation, produced highly active mixed oxides for transesterification and acetone coupling. However, if crystalline ZrO_2 at the surface of the oxide is detrimental to a reaction, the rising pH method of precipitation is the preferred synthesis procedure since crystalline ZrO_2 is buried below the interface.

Experimental Methods

Catalyst Synthesis

Rising pH Precipitation

The following method, which is based on the work of Aramendia et al.,[7] was used to prepare pure metal oxide and mixed metal oxide. First, 51 g of magnesium nitrate hexahydrate (Acros Organics, 98%) was dissolved in 1,000 cm^3 of distilled, deionized water. An appropriate amount of zirconyl nitrate hydrate (Acros Organics, 99.50%) was also dissolved in the solution to give the desired ratio of Mg:Zr. For example, to prepare a sample with a nominal 11:1 molar ratio of Mg to Zr (Mg:Zr 11:1), 4 g of zirconyl nitrate hydrate was dissolved. The oxide was then precipitated by the dropwise addition of 25 wt.% NaOH solution (Mallinckrodt Chemicals, 98.8%). Sodium hydroxide solution was added until the metal oxide solution reached a pH of 10. The mixture was then allowed to age for 72 h, after which it is was filtered and dried in air at 413 K. Subsequently, the catalyst was washed with water to remove Na, and calcined at 773 K in 100 cm^3 min^{-1} of flowing ultra-high purity dioxygen (Praxair, ultra-high purity) for 3 h.

Controlled pH Precipitation

Two separate aqueous solutions were fed to a continuously-stirred Labmax reactor. The first solution contained 1M NaOH solution, whereas the second one contained magnesium nitrate hexahydrate and zirconyl nitrate hydrate in appropriate concentrations. For example, to prepare a sample with a nominal 11:1 ratio of Mg:Zr (Mg:Zr 11:1), a solution of 76.47 g of magnesium nitrate and 6.05 g of zirconyl nitrate dissolved in 500 cm^3 of distilled, deionized water was used. This mixed metal salt solution was fed to the Labmax reactor at a rate of 4.5 g min^{-1}, which had an initial volume of 400 cm^3 of distilled, deionized water and NaOH at an initial pH of 11. The solution was fed continuously until 390 grams had been pumped into the reactor. The NaOH

solution was used to maintain the solution pH in the reactor at a constant value of 10.5 (This was the lowest value of pH that could be accurately controlled in this precipitation). The resulting solid was aged for 72 h, filtered, dried at in air 403 K, washed with water to remove Na, and calcined at 773 K in 100 cm^3 min^{-1} of flowing dioxygen.

Magnesia Supported onto Zirconia

An additional set of catalysts was prepared to investigate the role of zirconia as a support for magnesia. First, zirconia was precipitated using the rising pH method, dried, washed, and calcined as described above. Second, a specified amount of zirconia was added to a solution with 51 g of magnesium nitrate. Sodium hydroxide was then added to the solution until a pH of 10 was achieved. The resulting solid was then aged for 72 h, filtered, dried, calcined and washed identically to the metal oxides described above.

Catalyst Characterization

The elemental analysis (Zr, Mg, and Na) was performed by Galbraith Laboratories (2323 Sycamore Drive, Knoxville, TN 37921) using inductively coupled plasma optical emission spectrometry (ICP-OES).

Adsorption of N_2 was performed on a Micromeritics ASAP 2020 automated adsorption system to obtain the BET surface areas of the catalysts after evacuation at 723 K for 4 h.

The X-ray diffraction patterns were recorded on a PANalytical X'pert diffractometer using Cu K-α radiation.

Adsorption microcalorimetry experiments were completed on the same home built instrument that has been described previously by Bordawekar et al.[38,39,60,61] The instrument is a heat flow calorimeter with two cells that are inserted into a large aluminum block maintained at

303 K. One cell functioned as a sample cell and the other one served as a reference. A catalyst sample was first heated to 773 K under vacuum to a pressure less than 10^{-2} Pa. The sample was then cooled and allowed to thermally equilibrate with the system for 2 h prior to adsorption of carbon dioxide or ammonia. Initial dosing pressures of adsorbate ranged from 10 Pa to 600 Pa, and each dose was allowed to equilibrate with the sample for 15 min.

Scanning electron microscopy (SEM) and energy dispersive X-ray analysis (EDX) were performed with a Hitachi S-4800 (FEG) equipped with an EDAX Sapphire detector on an EDAX Genesis 4000 system. The samples were loosely dispersed on an Al-stub with conductive carbon glue to preserve the as-prepared morphology as much as possible. The micrographs were taken in secondary electron and low angle back scattered electron mode with an accelerating voltage of 2 kV or 15 kV.

Transesterification of Tributyrin with Methanol

The catalytic transesterification reactions were performed in a round bottom flask at 333 K with an overhead stirrer. The reactor was equipped with a reflux condenser and was continuously purged with flowing N_2 (Praxair, ultra-high purity and additionally purified by passage through a Supelco OMI-2 purifier) at 40 cm^3 min^{-1}. Methanol (Fisher, 99.9%) and tributyrin (Acros 98%) were used as reactants. In each run, 136.5 g of methanol and 43.8 g of tributyrin were loaded into the reactor with 6.5 g of dibutyl ether (Aldrich, 99.3%) as an internal standard. After the temperature of the reactants reached 333 K, 0.5 to 1 g of the catalyst, which was first heat treated at 773 K for 1 h in flowing purified N_2, was added to the reactants to initiate the transesterification. The catalyst was directly transferred to the reactor to avoid CO_2 contamination from air. Liquid samples were removed from the reactor at different time intervals

and analyzed for products using an Agilent 5890 gas chromatograph equipped with a DB-5 capillary column.

The transesterification of tributyrin (T) with methanol (M) proceeds in three consecutive steps as shown in the following reaction sequence:

$$T + M \xrightarrow{k_1} D + MB \quad (1)$$

$$D + M \xrightarrow{k_2} Mo + MB \quad (2)$$

$$Mo + M \xrightarrow{k_3} G + MB \quad (3)$$

where D, MB, Mo and G denote dibutyrin, methyl butyrate, monobutyrin and glycerol, respectively. The reaction was assumed to be essentially irreversible and pseudo first order because of the large of excess of methanol. The pseudo first order kinetic model with respect to the butyrin components was used here to quantify the reaction rate constants on a surface area basis k_1, k_2, k_3 (L mol^{-1} m^{-2} min^{-1}) and the deactivation parameter α (min^{-1}). This is the same procedure that has been described in detail in previous works,[4,40,42,62] however, only k_1 is reported here.

Acetone Coupling

Acetone coupling was carried out in a round bottom flask maintained at 299 K. The 150 cm^3 reactant solution consisted of 95 wt.% acetone (Sigma-Aldrich, $\geq$99.9%) and 5 wt.% hexane (Sigma-Aldrich, $\geq$97%) as an internal standard. The acetone solution was rapidly stirred with a magnetic stir bar. After the temperature of the reactant reached 299 K, a thermally-pretreated catalyst (773 K for 1 h in flowing purified N_2) was added to the reactor without exposure to air to initiate the coupling reaction. The amount of catalyst used was adjusted to give 40 m^2 of surface

area and the reactor was initially purged for 10 minutes with 100 cm^3 min^{-1} of purified dinitrogen prior to addition of the catalyst. Samples of the product were taken at different time intervals and analyzed with an Agilent gas chromatograph equipped with a DB-WAX column. The initial rates of acetone coupling were calculated by producing a linear fit to the production of diacetone alcohol over the first 30 minutes of reaction. The selectivity to diacetone alcohol was >99% and conversion of acetone was between 1 and 2%. The rates presented here were normalized to surface area of catalyst added to the reaction.

Acetone Condensation

Acetone condensation was carried out in a gas phase, downward flow, fixed bed reactor. The feed to the reactor, 95 wt.% acetone (Sigma-Aldrich, $\geq$99.9%) and 5 wt. % hexane (Sigma-Aldrich, $\geq$97%) as an internal standard, was pumped to a vaporizer at a rate of 0.02 cm^3 (liquid) min^{-1}. The acetone/hexane vapor was then mixed with 100 cm^3 min^{-1} flowing He to give 5.5 % acetone in the vapor stream. All gas lines were maintained at 473 K to avoid condensation of reactants and products. The feed mixture flowed through the catalyst bed and then into a gas sampling valve for online gas chromatography. This reaction was performed at less than 103.4 kPa gauge and at 573 K. A constant surface area of metal oxide catalyst, 14 m^2 g^{-1}, was loaded into the fixed bed reactor. Product analysis was carried out with an Agilent 7890 GC equipped with a DB-WAX column.

Dehydration and Dehydrogenation of Ethanol

Conversion of ethanol was carried out in a gas phase, downward flow, fixed bed reactor. A reactant stream of ethanol (Sigma-Aldrich, 99.5% purity anhydrous) and 5 wt.% octane (Sigma-Aldrich, 99.9% purity anhydrous) as an internal standard was fed to a vaporizer that

contained glass beads and 3 Å molecular sieves to remove water from the ethanol feed. The ethanol and octane mixture was vaporized and mixed with flowing N_2 to give 6.8 % ethanol in the vapor stream. The vaporizer was maintained at 333 K and all gas lines were maintained at 473 K to avoid condensation of reactants and products. The feed mixture flowed through the catalyst bed and then into a gas sampling valve for online gas chromatography. The GC column was a Varian CP-Poraplot column, 25 m in length with an internal diameter of 0.32 mm. The reaction was performed between 136 to 170 kPa absolute and at 673 K. The flow rate of N_2 and reactant liquid was 100 cm^3 min^{-1} and 0.02 cm^3 min^{-1} respectively.

Acknowledgements

This work was supported by the Chemical Sciences, Geosciences and Biosciences Division, Office of Basic Energy Sciences, Office of Science, U.S. Department of Energy, grant no. DE-FG02-95ER14549 and NSF grant number OISE 0730277. Scanning electron microscopy was performed by Gisele Weinberg.

References

[1] S. Liu, X. Zhang, J. Li, N. Zhao, W. Wei, Y. Sun, *Catal. Commun.* **2008**, *9*, 1527–1532.

[2] I. Sádaba, M. Ojeda, R. Mariscal, R. Richards, M. L. L. Granados, *Catal. Today* **2010**, *167*, 77–83.

[3] I. Sádaba, M. Ojeda, R. Mariscal, J. L. G. Fierro, M. L. Granados, *Appl. Catal. B:Environ.* **2011**, *101*, 638–648.

[4] J. T. Kozlowski, M. T. Aronson, R. J. Davis, *Appl. Catal. B:Environ.* **2010**, *96*, 508–515.

[5] R. Sree, N. S. Babu, P. S. Prasad, N. Lingaiah, *Fuel Process. Technol.* **2009**, *90*, 152–157.

[6] K. Tanabe, T. Yamaguchi, *Catal. Today* **1994**, *20*, 185–197.

[7] M. A. Aramendía, V. Boráu, C. Jiménez, A. Marinas, J. M. Marinas, J. A. Navio, J. R. Ruiz, F. J. Urbano, *Colloids Surf., A* **2004**, *234*, 17–25.

[8] M. A. Aramendía, V. Borau, C. Jiménez, J. M. Marinas, J. R. Ruiz, F. J. Urbano, *Appl. Catal. A:Gen.* **2003**, *244*, 207–215.

[9] C. J. Barrett, J. N. Chheda, G. W. Huber, J. A. Dumesic, *Appl. Catal. B:Environ.* **2006**, *66*, 111–118.

[10] M. A. Aramendía, V. Boráu, C. Jiménez, J. M. Marinas, A. Marinas, A. Porras, F. J. Urbano, *J. Catal.* **1999**, *183*, 240–250.

[11] M. A. Aramendía, V. Borau, C. Jiménez, A. Marinas, J. M. Marinas, J. R. Ruiz, F. J. Urbano, *J. Mol. Catal. A: Chem.* **2004**, *218*, 81–90.

[12] J. Tai, R. J. Davis, *Catal. Today* **2007**, *123*, 42–49.

[13] M. J. Climent, A. Corma, V. Fornés, R. Guil-Lopez, S. Iborra, *Adv. Synth. Catal.* **2002**, *344*, 1090–1096.

[14] J. I. Di Cosimo, C. R. Apesteguía, M. J. L. Ginés, E. Iglesia, *J. Catal.* **2000**, *190*, 261–275.

[15] E. Iglesia, D. G. Barton, J. A. Biscardi, M. J. L. Gines, S. L. Soled, *Catal. Today* **1997**, *38*, 339–360.

[16] S. Huber, H. Knozinger, *J. Mol. Catal. A-Chem.* **1999**, *141*, 117–127.

[17] J. Lercher, H. Noller, G. Ritter, *J. Chem. Soc. Faraday Trans.* **1981**, *1*, 621–628.

[18] D. Cornu, H. Guesmi, J. Krafft, H. Lauron-Pernot, *J. Phys. chem. C* **2012**, *116*, 6645–6654.

[19] M. Bensitel, O. Saur, J. Lavalley, *Mater. Chem. Phys.* **1991**, *28*, 309–320.

[20] M. A. Hasan, M. I. Zaki, L. Pasupulety, *J. Mol. Catal. A-Chem.* **2002**, *178*, 125–137.

[21] C. Pighini, T. Belin, J. Mijoin, P. Magnoux, G. Costentin, H. Lauron-Pernot, *Appl. Surf. Sci.* **2011**, *257*, 6952–6962.

[22] A. Auroux, A. Gervasini, *J. Phys. Chem.* **1990**, *94*, 6371–6379.

[23] C. Chizallet, M. L. Bailly, G. Costentin, H. Lauron-Pernot, J. M. Krafft, P. Bazin, J. Saussey, M. Che, *Catal. Today* **2006**, *116*, 196–205.

[24] M. Bailly, C. Chizallet, G. Costentin, J. Krafft, H. Lauron-Pernot, M. Che, *J. Catal.* **2005**, *235*, 413–422.

[25] R. Vidruk, M. V. Landau, M. Herskowitz, M. Talianker, N. Frage, V. Ezersky, *J. Catal.* **2009**, *263*, 196–204.

[26] A. O. Menezes, P. S. Silva, E. P. Hernández, L. E. P. Borges, M. A. Fraga, *Langmuir* **2010**, *26*, 3382–7.

[27] H. Lauron-Pernot, *Catal. Rev.* **2006**, *48*, 315–361.

[28] J. M. Montero, P. Gai, K. Wilson, A. F. Lee, *Green Chem.* **2009**, *11*, 265.

[29] K. Zhu, J. Hu, C. Kübel, R. Richards, *Angew. Chem. Int. Ed.* **2006**, *45*, 7277–81.

[30] J. F. Sanz, J. Oviedo, A. Márquez, J. A. Odriozola, M. Montes, *Angew. Chem. Int. Edit.* **1999**, *38*, 506–509.

[31] M. M. Branda, A. H. Rodríguez, P. G. Belelli, N. J. Castellani, *Surf. Sci.* **2009**, *603*, 1093–1098.

[32] H. Kawakami, Y. Satohiro, *J. Chem. Soc., Faraday Trans.* **1984**, 921–932.

[33] R. Kakkar, P. N. Kapoor, K. J. Klabunde, *J. Phys. Chem. B* **2004**, *108*, 18140–18148.

[34] M. M. Branda, P. G. Belelli, R. M. Ferullo, N. J. Castellani, *Catal. Today* **2003**, *85*, 153–165.

[35] H. Petitjean, K. Tarasov, F. Delbecq, P. Sautet, J. M. Krafft, P. Bazin, M. C. Paganini, E. Giamello, M. Che, H. Lauron-Pernot, et al., *J. Phys. Chem. C* **2010**, *114*, 3008–3016.

[36] C. A. Ferretti, S. Fuente, R. Ferullo, N. Castellani, C. R. Apesteguía, J. I. Di Cosimo, *Appl. Catal. A:Gen.* **2012**, *413-414*, 322–331.

[37] J. L. Anchell, K. Morokuma, A. C. Hess, *J. Chem. Phys.* **1993**, *99*, 6004.

[38] S. V. Bordawekar, R. J. Davis, *J. Catal.* **2000**, *189*, 79–90.

[39] S. V. Bordawekar, E. J. Doskocil, R. J. Davis, *Langmuir* **1998**, *14*, 1734–1738.

[40] Y. Xi, R. J. Davis, *J. Catal.* **2009**, *268*, 307–317.

[41] D. E. López, J. G. Goodwin Jr., D. A. Bruce, E. Lotero, *Appl. Catal. A:Gen.* **2005**, *295*, 97–105.

[42] Y. Xi, R. J. Davis, *Clay. Clay Miner.* **2010**, *58*, 475–485.

[43] S. Abelló, F. Medina, D. Tichit, J. Pérez-Ramírez, J. C. Groen, J. E. Sueiras, P. Salagre, Y. Cesteros, *Chem. Eur. J.* **2005**, *11*, 728–39.

[44] N. E. Fouad, P. Thomasson, H. Knözinger, *Appl. Catal. A:Gen.* **2000**, *196*, 125–133.

[45] C. Ma, G. Liu, Z. Wang, Y. Li, J. Zheng, W. Zhang, M. Jia, *React. Kinet. Catal. Lett.* **2009**, *98*, 149–156.

[46] P. Kustrowski, D. Sulkowska, L. Chmielarz, A. Rafalskalasocha, B. Dudek, R. Dziembaj, *Microporous Mesoporous Mater.* **2005**, *78*, 11–22.

[47] J. I. Di Cosimo, V. K. Díez, C. R. Apesteguía, *Appl. Catal. A:Gen.* **1996**, *137*, 149–166.

[48] P. Thomasson, O. S. Tyagi, H. Knözinger, *Appl. Catal. A:Gen.* **1999**, *181*, 181–188.

[49] C. Carlini, M. Marchionna, M. Noviello, A. M. R. Galletti, G. Sbrana, F. Basile, A. Vaccari, *J. Mol. Catal. A-Chem.* **2005**, *232*, 13–20.

[50] C. Carlini, C. Flego, M. Marchionna, M. Noviello, A. M. R. Galletti, G. Sbrana, F. Basile, A. Vaccari, *J. Mol. Catal. A-Chem.* **2004**, *220*, 215–220.

[51] W. Ueda, T. Kuwabara, T. Ohshida, Y. Morikawa, *J. Chem. Soc. Chem. Commun.* **1990**, 1558–1559.

[52] A. S. Ndou, N. J. Coville, *Appl. Catal. A:Gen.* **2004**, *275*, 103–110.

[53] A. S. Ndou, N. Plint, N. J. Coville, *Appl. Catal. A:Gen.* **2003**, *251*, 337–345.

[54] M. J. L. Gines, E. Iglesia, *J. Catal.* **1998**, *176*, 155–172.

[55] T. Tsuchida, S. Sakuma, T. Takeguchi, W. Ueda, *Ind. Eng. Chem.* **2006**, *45*, 8634–8642.

[56] T. Tsuchida, J. Kubo, T. Yoshioka, S. Sakuma, T. Takeguchi, W. Ueda, *J. Catal.* **2008**, *259*, 183–189.

[57] Y. Zhao, W. Li, M. Zhang, K. Tao, *Catal. Commun.* **2002**, *3*, 239–245.

[58] A. A. Tsyganenko, D. V. Pozdnyakov, V. N. Filimonov, *J. Mol. Struct.* **1975**, *29*, 299–318.

[59] M. Zaki, M. Hasan, L. Pasupulety, *Langmuir* **2001**, *17*, 768–774.

[60] E. J. Doskocil, S. V. Bordawekar, R. J. Davis, *J. Catal.* **1997**, *169*, 327–337.

[61] S. V. Bordawekar, E. J. Doskocil, R. J. Davis, *Catal. Lett.* **1997**, *44*, 193–199.

[62] Y. Xi, R. J. Davis, *Inorg. Chem.* **2010**, *49*, 3888–95.

Table 1. Results from N_2 adsorption and elemental analysis.

Catalyst	Synthesis Method or Source	Surface Area (m^2 g^{-1})	Mg Content on a Metals Basis (Mg/(Mg+Zr))	Na Content (ppm)
Mg:Zr 1:1[(a)]	Rising pH Precipitation	176	0.58	<100
Mg:Zr 5:1[(a)]	Rising pH Precipitation	223	0.85	<100
Mg:Zr 8:1[(a)]	Rising pH Precipitation	256	0.89	<100
Mg:Zr 11:1[(a)]	Rising pH Precipitation	173	0.92	<100
Mg:Zr 11:1	Controlled pH Precipitation	194	0.94	<100
Mg on Zr 11:1	Rising pH Precipitation	291	0.93	340
MgO[(a)]	Rising pH Precipitation	292	1.00	<100
MgO	Controlled pH Precipitation	162	1.00	<100
MgO[(a)]	from $Mg(OH)_2$ Sigma Aldrich	22	1.00	-
MgO	Ube MgO 500 Å	35	1.00	-
ZrO_2[(a)]	Rising pH Precipitation	123	N/A	100
ZrO_2	Controlled pH Precipitation	70	N/A	340
ZrO_2	Sigma Aldrich	13	N/A	220

(a) Results presented in Kozlowski et al.[4]

Table 2. Summary of results from adsorption microcalorimetry of ammonia and carbon dioxide on Mg and Zr containing oxides.

	NH_3 Adsorption		CO_2 Adsorption	
Catalyst	Initial -ΔH (kJ mol^{-1})	Coverage (μmol m^{-2})	Initial -ΔH (kJ mol^{-1})	Coverage (μmol m^{-2})
MgO[(a)]	120	0.70	162	0.83
Mg:Zr 11:1[(b)]	84	0.73	185	0.74
Mg:Zr 11:1[(a)]	141	0.73	187	0.91
Mg:Zr 5:1[(b)(c)]	-	-	154	1.2
Mg on Zr 11:1[(b)]	-	-	153	1.0
ZrO_2 [(a)]	170	3.5	123	0.81

(a) Sample prepared by controlled pH precipitation

(b) Sample prepared by rising pH precipitation

(c) Result presented in Kozlowski et al.[4]

Table 3. Rate constants for transesterification of tributyrin with methanol at 333 K over pure and mixed oxides of zirconia and magnesia.

Catalyst	k_1 ($x10^6$)[(e)] ($L\ mol^{-1}\ m^{-2}\ s^{-1}$)
Mg:Zr 1:1[(a)(b)]	0.37 ± 0.12
Mg:Zr 5:1[(a)(b)]	0.50 ± 0.03
Mg:Zr 8:1[(a)(b)]	0.73 ± 0.07
Mg:Zr 11:1[(a)(b)]	3.0 ± 0.30
Mg:Zr 11:1[(c)]	3.2 ± 0.35
Mg on Zr 11:1[(b)]	0.66 ± 0.13
MgO[(a)(b)]	0.70 ± 0.02
MgO from $Mg(OH)_2$[(a)(d)]	1.2 ± 0.34
ZrO_2[(b)]	0

(a) Result presented in Kozlowski et al.[4]
(b) Sample prepared by titration precipitation
(c) Sample prepared by controlled pH precipitation
(d) $Mg(OH)_2$, nanopowder (Aldrich, 99.9%)
(e) Rate constant for consumption of tributyrin (or rate of dibutryrin production) normalized to surface area of catalyst

Table 4. Rates of diacetone production over the pure oxides, the controlled pH precipitation and the rising pH precipitation samples.

Catalyst	Rate of Diacetone Alcohol Production (mol s^{-1} m^{-2})(x10^7) [c]	TOF (s^{-1})[d]
Mg:Zr 11:1[a]	1.6	0.21
Mg:Zr 11:1[b]	1.7	0.19
Mg:Zr 5:1[a]	1.2	0.10
Mg on Zr 11:1[a]	1.2	0.12
MgO[b]	0.81	0.10
ZrO_2[b]	0.00	N/A

(a) Mixed oxides prepared by rising pH precipiation
(b) Samples prepared by controlled pH precipitation
(c) Rates were calculated from the first 30 minutes of reaction.
(d) TOF was calculated by normalizing the rate by the CO_2 adsorption capacity.

Table 5. Conversion and selectivities for acetone condensation in a flow reactor at 573 K.

Catalyst	Initial Conversion[(e)]	Conversion at 12 hours [(e)]	Mesityl Oxide Selectivity	Isophorone Selectivity	Mesitylene Selectivity
ZrO_2 (S.A.)[(a)]	10%	9%	80%	8%	12%
Mg:Zr 1:1[(b)]	7%	3%	82%	14%	4%
Mg:Zr 5:1[(b)]	5%	3%	78%	6%	16%
Mg:Zr 11:1[(c)]	5%	2%	85%	4%	11%
MgO[(d)]	12%	5%	80%	19%	trace

(a) ZrO_2 obtained from Sigma-Aldrich
(b) Mixed oxides prepared by rising pH precipitation, same materials discussed in Kozlowski et al.[4]
(c) Controlled pH precipitation sample
(d) MgO obtained from Ube Material Industries Ltd. (Ube MgO 500Å)
(e) Conversion calculated by the sum of all products that were identified and quantified (diacetone alcohol, mesityl oxide, isophorone, and mesitylene).

Table 6. Ethanol reaction rates to ethene, ethanal and butanol at 673 K.

Catalyst	Ethene Formation Rate (mol m^{-2} s^{-1}) $x10^9$	Ethanal Formation Rate (mol m^{-2} s^{-1}) $x10^9$	Butanol Formation Rate (mol m^{-2} s^{-1}) $x10^9$
MgO[(a)]	6.6	15	1.1
Mg:Zr 11:1[(b)]	12	15	0.8
Mg:Zr 11:1[(a)]	19	19	N.O.[(c)]
ZrO_2[(a)]	180	10	N.O.[(c)]

(a) Sample prepared by controlled pH precipitation

(b) Sample prepared by rising pH precipitation

(c) Butanol was not detected in the products

Table 7. Turnover frequencies for ethanol dehydration and dehydrogenation to ethene and ethanal, respectively.

Catalyst	Ethene TOF (s^{-1})[(c)]	Ethanal TOF (s^{-1})[(d)]
MgO[(a)]	0.009	0.018
Mg:Zr 11:1[(b)]	0.016	0.021
Mg:Zr 11:1[(a)]	0.025	0.020
ZrO_2[(a)]	0.051	0.012

(a) Sample prepared by controlled pH precipitation
(b) Sample prepared by rising pH precipitation
(c) Rate of ethene production divided by ammonia uptake measured by adsorption microcalorimetry
(d) Rate of ethanal production divided by carbon dioxide uptake measured by adsorption microcalorimetry

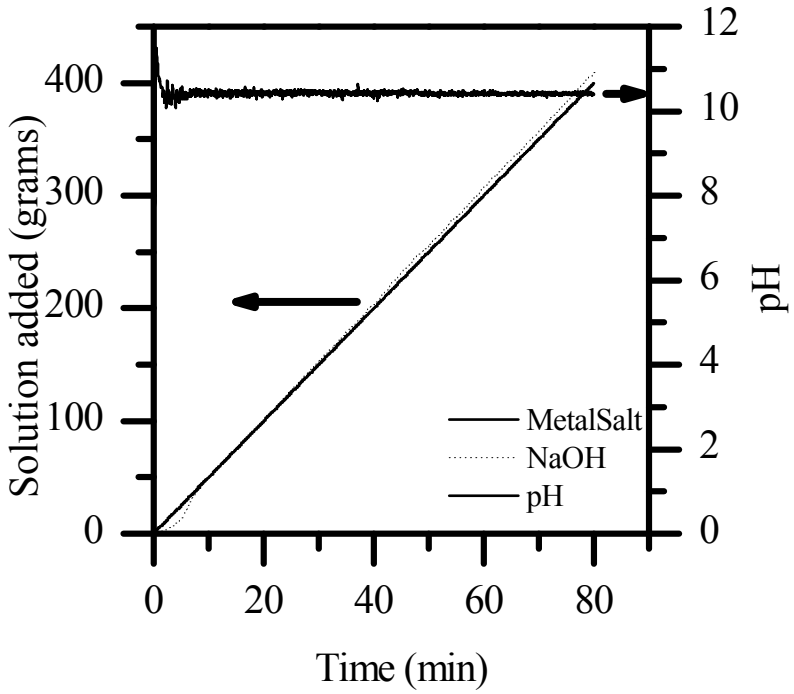

Figure 1. The pH of the slurry containing precipitate (Mg:Zr 11:1) as sodium hydroxide and metal precursor were continuously added to the Labmax reactor. (--) grams of 1 M NaOH(aq) solution added, (-) grams of metal salt precursor solution added, (-) pH of solution

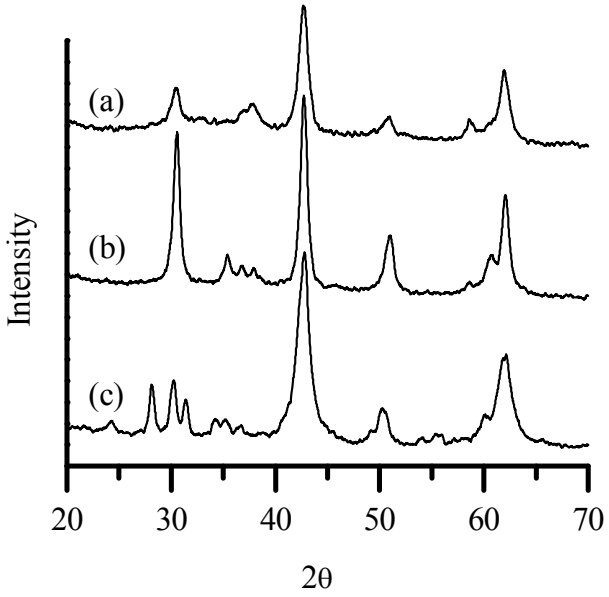

Figure 2. X-ray diffraction patterns of: (a) controlled precipitated 11:1 Mg:Zr mixed oxide, (b) rising pH precipitated 11:1 Mg:Zr mixed oxide, and (c) Mg on Zr 11:1 mixed oxide.

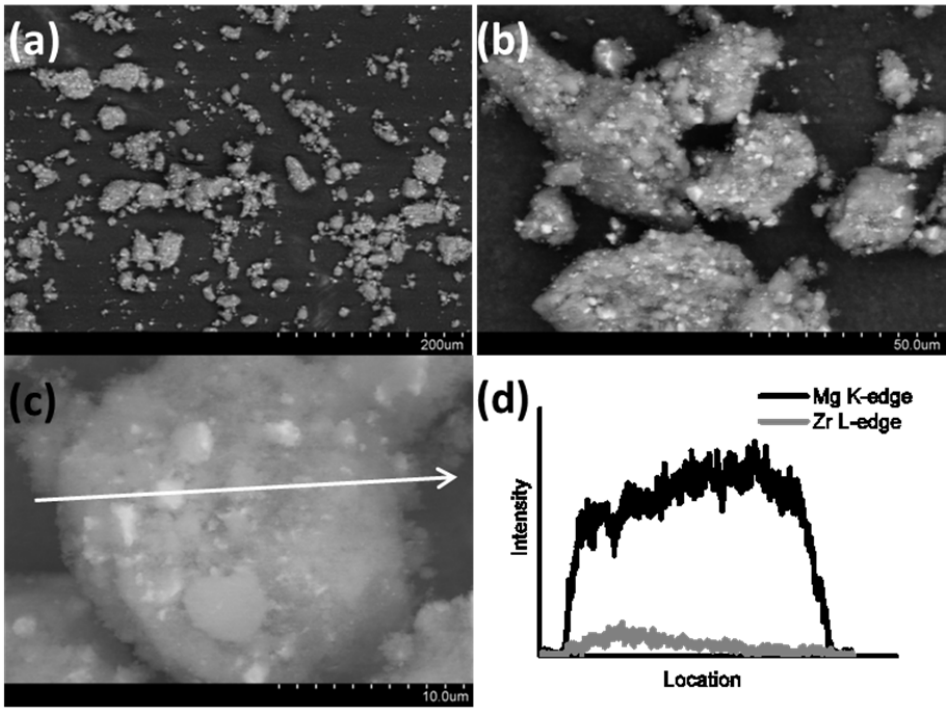

Figure 3. SEM images (a), (b) and (c) of the controlled precipitation material. (d) EDX of the line scan whose direction is shown on image (c).

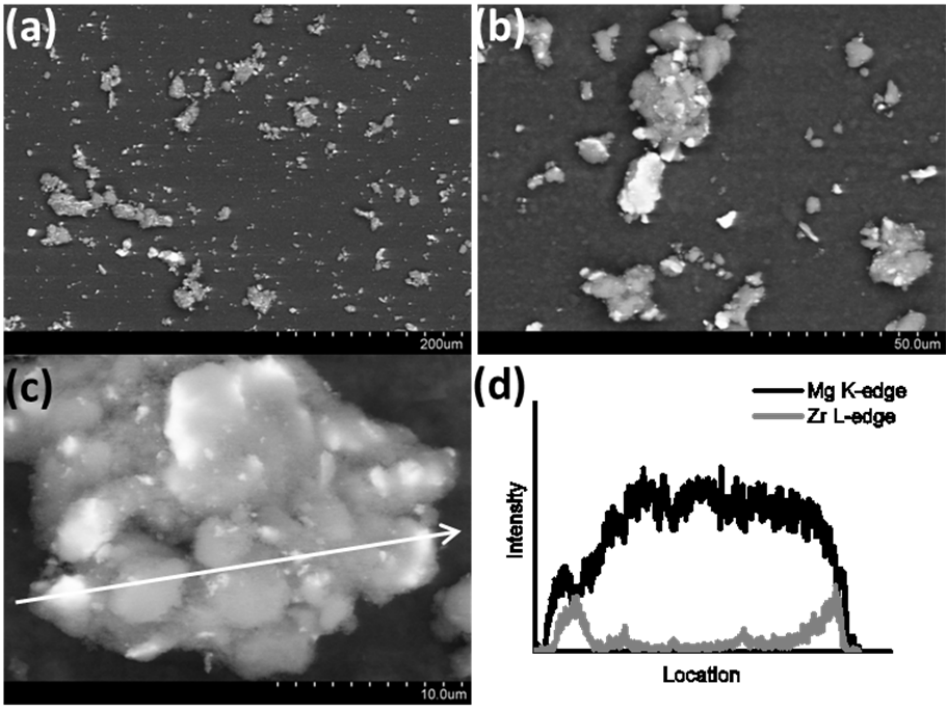

Figure 4. SEM images (a), (b) and (c) of the rising pH precipitation material. (d) EDX of the line scan whose direction is shown on image (c).

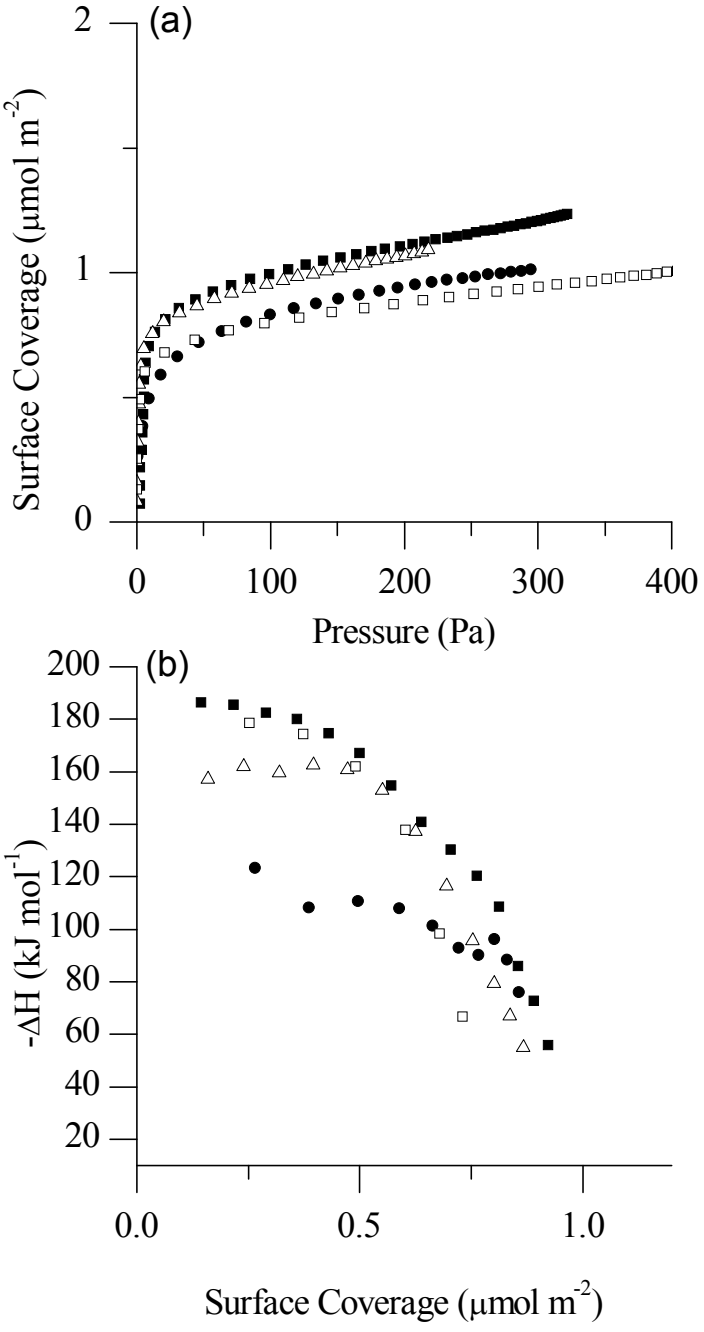

Figure 5. CO_2 adsorption microcalorimetry on controlled pH precipitated MgO (Δ), ZrO_2 and (●) Mg:Zr 11:1(■) with rising pH precipitation Mg:Zr 11:1 (□). (a) adsorption isotherm and (b) differential heats of adsorption

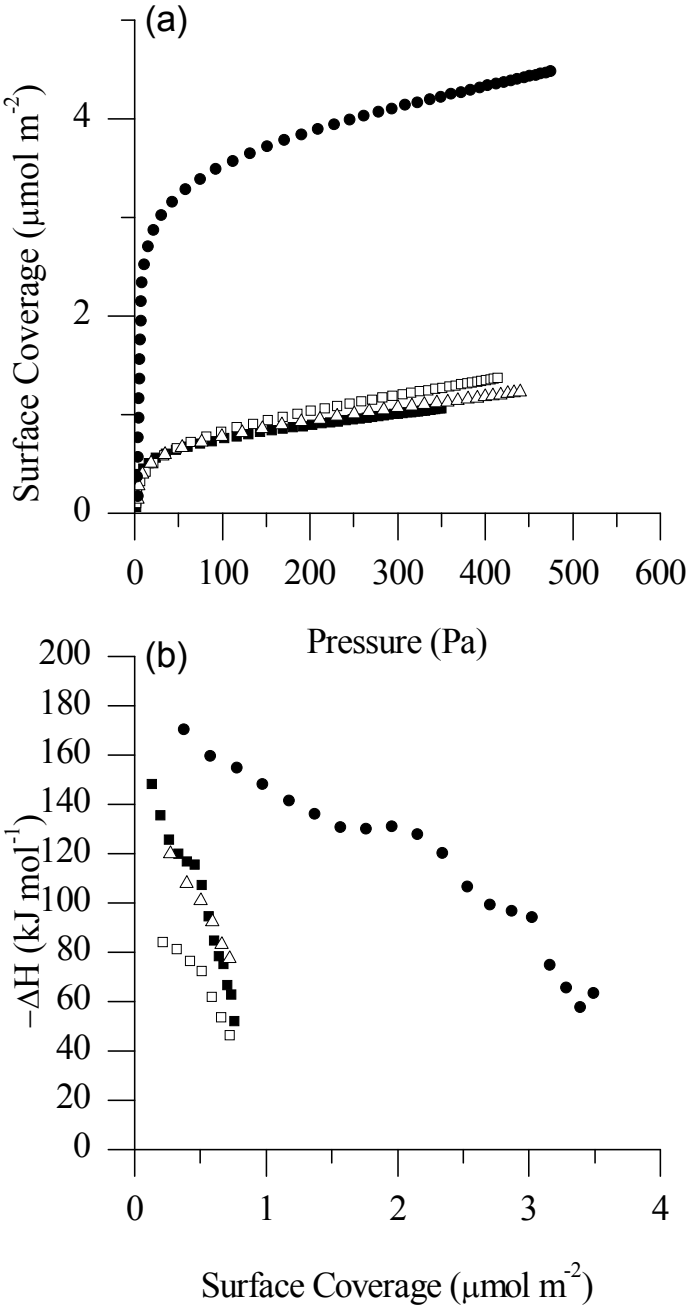

Figure 6. NH_3 adsorption microcalorimetry on controlled pH precipitated MgO (Δ), ZrO_2 and (●) Mg:Zr 11:1(■) with rising pH precipitation Mg:Zr 11:1 (□). (a) adsorption isotherm and (b) differential heats of adsorption

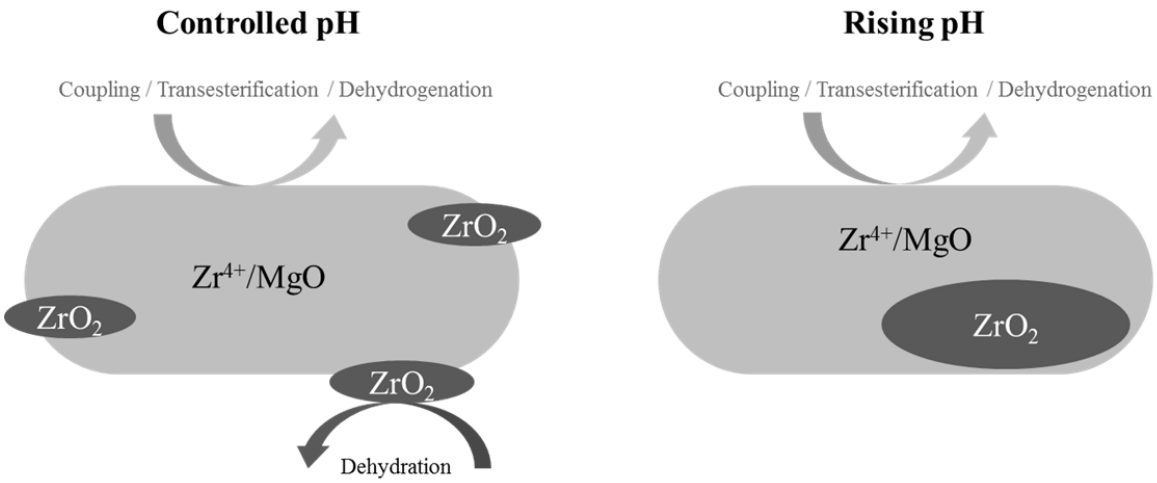

Figure 7. An illustration of the Mg:Zr 11:1 catalyst particles prepared using controlled pH (left) and rising pH (right) precipitation methods. The Zr^{4+}/MgO phase accelerates the rates of acetone coupling and tributyrin transesterification with methanol compared to unpromoted MgO. Although ethanol dehydrogenates on both ZrO_2 and MgO, dehydration is favored over ZrO_2.